Chalcogenide Letters Vol. 19, No. 10, October 2022, p. 691 - 699

Physical properties of Cu_2MgSnS_4 thin films prepared by chemical spray pyrolysis technique: The effect of thiourea concentration

Rafal A. Abdullah[a], Nabeel A. Bakr[a*], Kiran D. Diwate[b]
[a]*Department of Physics, College of Science, University of Diyala, Iraq*
[b]*Department of Physics, The P.G.K. Mandal's Haribhai V. Desai College, Pune 411002, India*

In this work, chemical spray pyrolysis is employed to prepare Cu_2MgSnS_4 thin films using different concentrations of thiourea (0.14, 0.16, 0.18, 0.20, 0.22, 0.24) M at a substrate temperature of 400 ℃ and thickness of (300±10) nm. The XRD results displayed that all thin films are polycrystalline with tetragonal structure and favorite orientation along the (112) plane. The crystallite size of films is estimated by Scherrer's equation and it was found that it increases with increasing thiourea concentration up to 0.20 M and then it decreases with further increase in thiourea concentration. The FESEM result exhibited the appearance of nanostructures with different particle sizes and shapes. The band gap was estimated using Tauc's relationship and it was found that the value of the band gap increases with increasing thiourea concentration from 1.68 eV at 0.14 M to 1.83 eV at 0.20 M and then it decreases to 1.60 eV at 0.24 M. Raman spectroscopy investigation confirms the purity of the sample formation phase. The main peak for all films is located at about 330 cm^{-1}. The broadening of this peak in solid solutions can be attributed to the disturbance effects related to the locations of the metal and sulfur atoms in the tetrahedral lattice due to chemical substitutions in the crystalline positions. Hall effect results showed that all films are P-type. The increase in carrier concentration and its motility with increasing thiourea concentrations leads to a decrease in the resistance of the films.

(Received August 1, 2022; Accepted October 7, 20222)

Keywords: Cu_2MgSnS_4 thin films, Chemical spray pyrolysis, Optical properties, Structural properties, Hall effect

1. Introduction

Nowadays energy has become a requirement for mankind. To deal with it, mostly we rely upon the energy resources like coal and petroleum. Thus the rapid growth in population, energy issues, and deterioration of environment has evolved as the main test for us [1]. The use of the fossil fuels has produced serious environmental concerns by emitting CO_2 upon combustion leading to a greenhouse effect. On account of these issues, renewable energy has now paved its techniques as a possible solution for the above problem. Solar energy has been reported as the most efficient among all the known renewable energy resources. The pioneering work of Fujishima and Honda opened up a broad research field to find suitable, stable semiconductors and inexpensive water splitting applications [2]. To make efficient use of this abundant solar energy through water splitting, several semiconductors have been taken under the trail to develop a suitable photo absorber material [3, 4]. But to see at least one-third of the projected energy requests of human society, we need materials with a minimum solar energy conversion efficiency of 10%. Copper-based chalcogenides possess a band gap value of 1.5 eV and thus are often regarded as a suitable alternate for generating energy. Between all, Cu_2ZnSnS_4 has been widely examined as a low-cost, earth-abundant photo absorber material. To date, it has been possible to achieve only Cu_2ZnSnS_4 (CZTS) and Cu_2ZnSnS_x/Se (CZTS/Se) based solar cells with an efficiency of 11 and 12:6,

* Corresponding author: nabeelalibakr@yahoo.com
https://doi.org/10.15251/CL.2022.1910.691

respectively [3]. The formation of antisite defects and impurity phases have been reported to be responsible for this limitation in efficiency. Thus, it has been proposed that replacing Zn with neighboring transition elements (e.g., Ni, Co, Fe, Mg, Cr) or group IIA elements (Ca, Mg, Ba, Sr) or group IIB elements (Hg, Cd) can eliminate these defects causing [2]. This work aims to use chemical spray pyrolysis method to prepare Cu_2MgSnS_4 (CMTS) films and to study the effect of thiourea concentrations on the structural, morphological, optical, and Hall effect properties of these films.

2. Experimental details

Chemical spray pyrolysis method is used to deposit Cu_2MgSnS_4 films on ordinary SLG substrates using high purity materials (99%). The required solutions are prepared using distilled water by mixing 0.04 M of copper chloride ($CuCl_2.2H_2O$), 0.02 M of tin chloride ($SnCl_4.5H_2O$), 0.02 M of magnesium chloride ($MgCl_4.6H_2O$) and the thiourea (CH_4N_2S) concentration was varied according to the values of 0.14, 0.16, 0.18, 0.20, 0.22 and 0.24 M. Equal volumes of the solutions were well mixed by magnetic stirrer and the final solution was left for 30 minutes to make sure that no residues are left. Filtered air is used as a carrier gas with a flow rate of roughly 5 ml/min. The deposition process was carried out using a homemade system at a substrate temperature of 400 ˚C. Other deposition parameters are described elsewhere [5].

The synthesized samples have a thickness of (~ 300 nm) as determined by gravimetric method. The structural properties were investigated by using Grazing Incidence X-Ray Diffractometer (Shimadzu XRD-6000) of Cu-Kα wavelength (1.5406 Å). Raman spectra were recorded in backscattering configuration using (Jobin-Yvon Horiba Labram 800). FESEM (MIRA3, TE-SCAN) was used to image the topography of the films' surface. The optical transmission and absorption spectra of the films were recorded by double beam Shimadzu UV-1800 spectrophotometer in the wavelength range of (350 – 900) nm. Hall effect measurements were conducted by using Ecopia HMS 3000 instrument.

3. Results and discussion

3.1. Results of XRD

XRD patterns of Cu_2MgSnS_4 (CMTS) thin films deposited at different thiourea concentrations of 0.14, 0.16, 0.18, 0.20, 0.22, and 0.24 M are shown in figure (1). Five clear diffraction peaks appeared in the XRD patterns of the films deposited at thiourea concentrations of 0.18 M and 0.20 M at $2\theta \sim 18.28^o$, 28.54^o, 32.9^o, 47.43^o and 56.18^o which correspond to the (002), (112), (200), (220) and (312) planes respectively which match well with the data of JCPDS card number (98-017-1983) confirming the formation of tetragonal structure and distinguished by high crystallinity from the rest of the films. On the other hand, only three peaks appear for the films deposited at thiourea concentrations of 0.14 M and 0.24 M at $2\Theta \sim 28.54°$, $47.43°$, $56.18°$, and four diffraction peaks appear for the films deposited at thiourea concentrations of 0.16 M and 0.22 M at $2\theta \sim 28.54^o$, 32.9^o, 47.43^o and 56.18^o. The strongest peak for all patterns is found at $\sim 28.54^o$, which is referred to the (112) plane. The XRD results at this direction are depicted in Table (1). The intensity of all peaks increases as the ratio of thiourea increases. One can observe also that as the concentration of thiourea increases, the peaks locations shift to lower angles until it reaches a concentration of 0.20 M, after that the peaks start to shift to higher angles as a result of irregular stresses in the crystal lattice caused by crystal defects. This shift may arise from the micro-strain induced when the additives are incorporated during the film growth. The broadening of the diffraction peaks is an indication of the nano size of prepared material, which is in agreement with the previous reported results reported by Dridi et al. [6].

The crystallite size (D), was calculated for the (112) plane by conventional Scherrer's formula [7]:

$$D = \frac{K\lambda}{\beta \cos\theta} \quad (1)$$

where (K) is constant and equal to 0.9, (λ) is the wavelength of incident X-ray radiation (1.5406 Å for CuK_{α}), (β) is the full width at half maximum of the peak, and (θ) is the Bragg's diffraction angle of the XRD peaks. The highest crystallite size was 8.78 nm for the sample deposited at thiourea concentration of 0.20 M. This concentration worked as a catalyst for crystal development, which in turn decreased the stress in lattice brought on by the nanosize effect. The crystallite size values are displayed in Table (1). The size of the crystallites increases with the increase in the concentration of thiourea until the thiourea concentration reaches 0.2 M, then the size of the crystallites decreases with the increase in the concentration of thiourea.

The following equation was used to compute the lattice parameters (a and c) [8]:

$$\frac{1}{d_{hkl}^2} = \frac{h^2+k^2}{a^2} + \frac{l^2}{c^2} \quad (2)$$

where (hkl) are Miller's indices and d_{hkl} is the inter-planar spacing.

The unit cell volume of all prepared samples is similar to or a little bigger than the standard volume (317.5 Å^3) where the unit cell suffered stress [9]. The values of the lattice constant for the films are in agreement with theoretical values found in the standard card of the material which are (a = 5.430 Å and c = 10.765 Å) and they are shown in Table (2). Since all samples' estimated lattice vector (c/2a) values are greater than the standard value (0.9912), the unit cell is extended in the c-direction.

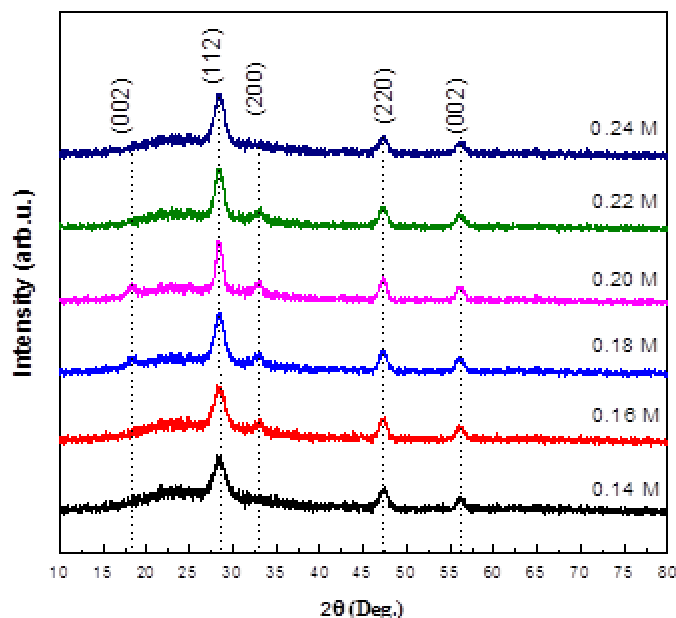

Fig. 1. XRD patterns of Cu_2MgSnS_4 thin films deposited at different concentrations of thiourea.

3.2. Raman Analysis

Raman shift measurements are analyzed to examine the phase purity of the deposited Cu_2MgSnS_4 thin films at different concentrations of thiourea and the result were plotted in figure (2). The spectra showed that they have a single broad peak at ~ 330 cm^{-1}. The broadening of this peak in solid solutions can be attributed to the disturbing effects related to the positions of the metal and sulfur atoms in the tetragonal lattice due to chemical substitutions at the crystalline positions [1,10]. This peak varies in intensity radiation from one sample to another. The sample deposited using 0.20 M of thiourea concentration displayed the highest intensity and the narrowest

full width at half maximum, and it also had the highest level of crystallization as shown in Table (3).

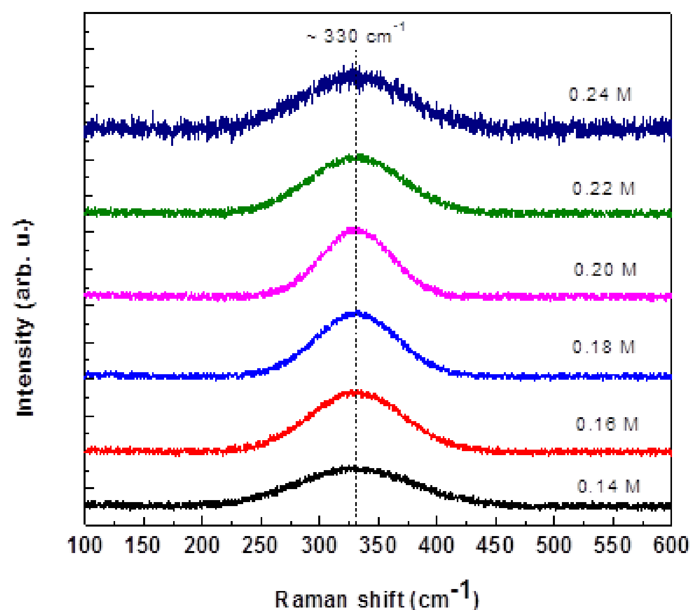

Fig. 2. Raman spectra of Cu_2MgSnS_4 thin films deposited at different concentrations of thiourea.

Table 1. XRD results of Cu_2MgSnS_4 thin films deposited at different concentrations of thiourea for the favorite growth direction (112).

	Thiourea Conc. (M)	2θ (Deg.)	FWHM (Deg.)	d (Å)	D (nm)
JCPDS	-	28.5300	-	3.1260	-
	0.14	28.5403	1.761	3.1250	4.7
	0.16	28.4455	1.451	3.1352	5.6
	0.18	28.3891	1.357	3.1413	6.0
	0.20	28.3667	0.933	3.1438	8.8
	0.22	28.4579	1.185	3.1339	6.9
	0.24	28.4579	1.382	3.1339	5.9

Table 2. Lattice parameters, unit cell volume and lattice vector values of Cu_2MgSnS_4 thin films deposited at different concentrations of thiourea.

	Thiourea Conc. (M)	a (Å)	c (Å)	V ($Å^3$)	c/2a
JCPDS	-	5.4300	10.7650	317.50	0.9912
	0.14	5.4172	10.8074	317.16	0.9975
	0.16	5.4194	10.9052	320.28	1.0061
	0.18	5.4272	10.9376	322.16	1.0077
	0.20	5.4282	10.9588	322.91	1.0094
	0.22	5.4238	10.8732	319.86	1.0024
	0.24	5.4211	10.8841	319.86	1.0039

Table 3. Results of Raman analysis of Cu_2MgSnS_4 thin films deposited at different concentrations of thiourea.

Thiourea Conc. **(M)**	Center of Peak **(cm^{-1})**	FWHM **(cm^{-1})**	Intensity **(arb. u.)**
0.14	326.4	118.9	5.9
0.16	329.2	88.3	8.5
0.18	330.2	85.5	8.9
0.20	329.2	67.3	9.7
0.22	329.7	97.4	8.3
0.24	328.7	102.7	9.0

3.3. FESEM Analysis

The FESEM images at 50 KX magnification of Cu_2MgSnS_4 thin films prepared by chemical spray pyrolysis technique at different concentrations of thiourea are shown in figure (3). The images reveal that films contain some voids and pores. It can be observed also that the prepared CMTS thin films have cauliflower-like forms with irregular particle sizes resulting from secondary growth on the surface and this indicates the growth of a new layer before the completion of the previous layer, which can be attributed to sulfur in excess of the specified value for the crystal structure of the compound. The stress caused due to drying of thin films are primarily responsible for crack generation. During heating, the lowermost layer of the film bound to the substrate does not relieve the stress due to the subsequent coatings, which is in agreement with other reports [2,6].

3.4. Optical properties

By employing UV–Vis spectrophotometry, the optical spectra of all films could be studied in the range of (300–900) nm to obtain precise information on the optical energy gap of films. The absorbance (A) as a function of wavelength is shown in figure (4). A fundamental absorption edge in the UV region of all films acted differently, shifting to a higher wavelength, refers to a narrow band gap caused by the increase in lattice defect and, consequently, the increase in absorbance. The absorbance increases until it reaches its maximum value at thiourea concentration of 0.2 M, and then it falls at greater concentrations of thiourea. Because local states exist close to the valence and conduction bands, the absorption edge is not sharp for all samples, which varies on the level of crystallization [11]. The density of grains in a particular area may differ from one sample to another depending on the size of the grains and the grains boundaries which may have different properties that can act as channels for scattering light. In addition, the presence of impurities near the grain regions leads to a large contrast between the grains and the boundaries, and this increases the scattering of light, and therefore the characteristics of the grain boundaries are important in determining the transparency of the material [12].

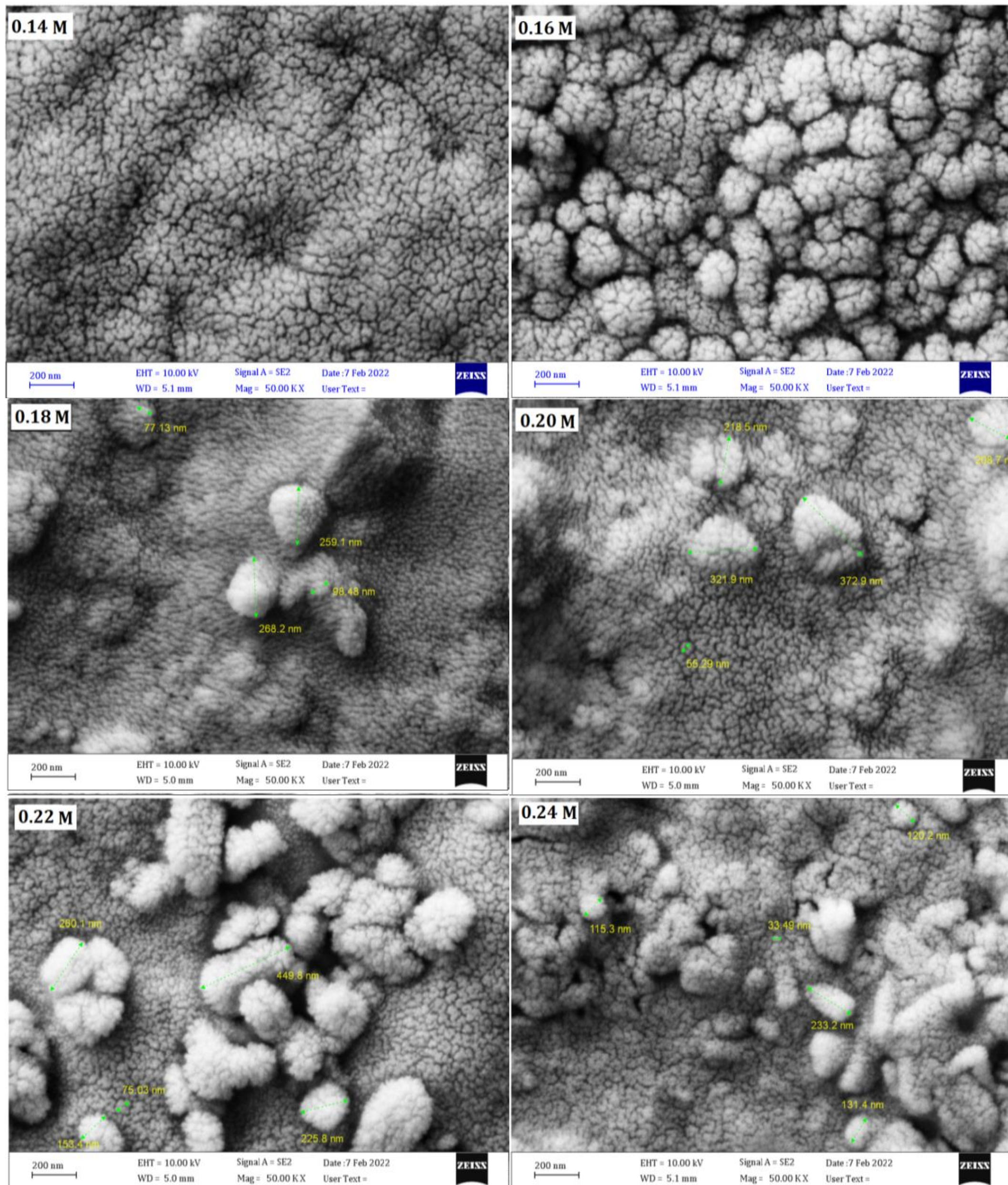

Fig. 3. FESEM images of Cu_2MgSnS_4 thin films deposited at different concentrations of thiourea.

The optical band gaps are estimated using the following formula [13,14]:

$$\alpha h v = B(h v - E_g)^r \quad (3)$$

where α is the coefficient of absorption, hν is the energy of photons, B is constant, and r has four numeric values (1/2) for allowed direct, 2 for allowed indirect, 3 for forbidden direct and (3/2) for forbidden indirect optical transitions. The optical band gap values are estimated by plotting a graphical relationship of $(\alpha h\nu)^2$ versus photon energy (hυ) and taking the best straight portion after the fundamental absorption edge to intersect the photon energy at $((\alpha h\nu)^2 = 0)$ as shown in figure (5). It can be seen that the value of the band gap increases with increasing thiourea concentration from 1.68 eV at 0.14 M to 1.83 eV at 0.20 M and then it decreases to 1.60 eV at 0.24 M as shown in table (4). The increase in the values of band gap can be attributed to the increase in the crystallization of the films and the reduction of crystal defects which lead to a decrease in the shallow local levels inside the forbidden gap which appears as an increase in the energy gap [15].

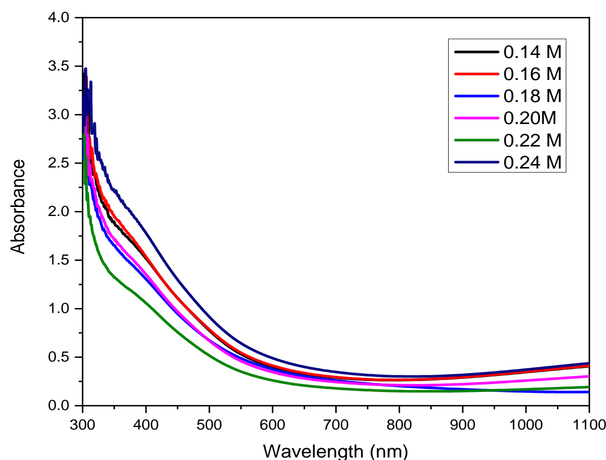

Fig. 4. Absorbance spectra of Cu_2MgSnS_4 thin films deposited at different concentrations of thiourea.

Table 4. Energy band gap of Cu_2MgSnS_4 thin films deposited at different concentrations of thiourea.

Thiourea Conc. **(M)**	Eg **(eV)**
0.14	1.68
0.16	1.69
0.18	1.77
0.20	1.83
0.22	1.80
0.24	1.60

3.5. Hall Effect

Hall Effect measurements results of Cu_2MgSnS_4 thin films deposited at different concentrations of thiourea are shown in table (5). The results show that all these films have a positive Hall coefficient (p-type charge carriers). The concentration of charge carriers increases with increasing thiourea concentration until it reaches 0.20 M and then the concentration of charge carriers decreases with further increase in thiourea concentration. The increase in carrier concentration and mobility as the thiourea concentrations increased leads to a decrease in the resistivity of films. According to the X-ray diffraction results, the increased carrier mobility as the thiourea concentration increases has been attributed to the increase in crystallite size [12].

Table 5. Hall measurements of Cu_2MgSnS_4 thin films deposited at different concentrations of thiourea.

Thiourea Conc. **(M)**	R_H **(cm^3/C)**	$n_H \times 10^{17}$ **(cm^{-3})**	μ_H **($cm^2/V.s$)**	ρ **(Ω.cm)**
0.14	11.75	5.31	4.122	2.852
0.16	8.69	7.18	5.127	1.696
0.18	6.85	9.11	6.992	0.98
0.2	5.29	11.8	8.023	0.659
0.22	6.32	9.88	6.954	0.908
0.24	7.68	8.13	5.861	1.31

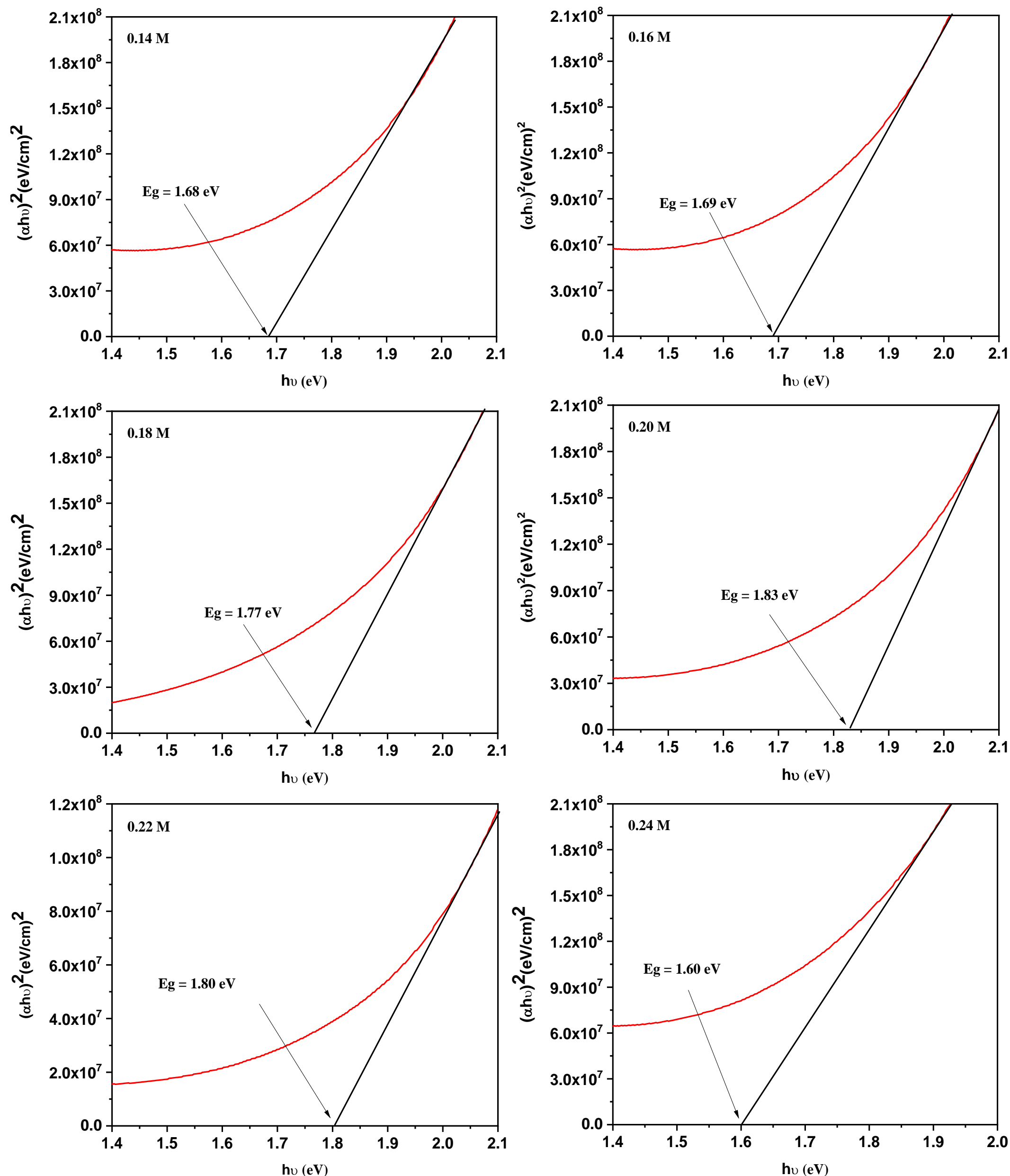

Fig. 5. Tauc's plots of Cu_2MgSnS_4 thin films deposited at different concentrations of thiourea.

4. Conclusions

Cu_2MgSnS_4 thin films deposited on glass substrates were successfully prepared by chemical spray pyrolysis technique. The X-ray diffraction results showed that all samples are polycrystalline and have a tetragonal structure. The films prepared at 0.20 M of thiourea had the highest crystallinity and the largest crystallite size. The Raman spectra showed one characteristic broad peak for all films located at about 330 cm^{-1}. The broadening of this peak in solid solutions can be attributed to the disturbance effects related to the locations of the metal and sulfur atoms in the tetrahedral lattice due to chemical substitutions in the crystalline positions.

FESEM images showed a difference in the surface nanostructures of the films, and images showed that the films were dense and rough and contained some voids and pores having cauliflower-like shapes. According to the optical properties, the energy gap values are associated with increased film crystallinity and reduced crystal defects. The film synthesized at 0.20 M of thiourea exhibits the highest optical energy gap value and the largest crystallite size. Hall effect

measurements showed that all films are of the same type and that the mobility of majority of carriers to increases with increasing thiourea concentration until it reaches 0.20 M concentration and then decreases with increasing thiourea concentration as a result of removing grain boundaries towards the charge carriers while enhancing sample crystallization. All films were of P-type and 0.20 M of thiourea concentration was the optimum value in terms of structural, electrical and optical properties. The properties of the prepared films indicate that they can be a good candidate for the absorbent layer in solar cells and other optoelectronics devices.

References

[1] A. Sharma, P. Sahoo, A. Singha, S. Padhan, G. Udayabhanu, and R. Thangavel, Sol. Energy, vol. 203, pp. 284–295, 2020; https://doi.org/10.1016/j.solener.2020.04.027
[2] A. Hammoud, B. Yahmadi, M. Souli, S. A. Ahmed, L. Ajili, and N. Kamoun-Turki, The European Physical Journal Plus, 137(2), 1-12, (2022); https://doi.org/10.1140/epjp/s13360-022-02417-z
[3] B. R. Bade, S. R. Rondiya, Y. A., Jadhav, M. M. Kamble, S. V. Barma, S. B. Jathar, and N. Y. Dzade, Journal of Alloys and Compounds, 854, 157093, (2021); https://doi.org/10.1016/j.jallcom.2020.157093
[4] A. Chavda, B. Patel, P. Marathey, I. Mukhopadhyay, and A. Ray, (2021), Materials Science and Engineering: B, 263, 114912, (2021); https://doi.org/10.1016/j.mseb.2020.114912
[5] N. A. Bakr, S. A. Salman, S. A. Hameed, International Journal of Applied Engineering Research 13(6), 3379 (2018).
[6] S. Dridi, E. Aubry, N. Bitri, F. Chaabouni, and P. Briois, Coatings, 10(10), 963, (2020); https://doi.org/10.3390/coatings10100963
[7] Z. T. Khodiar, N. F. Habubi, A. K. Abd, and A. M. Shano, Int. J. Nanoelectron. Mater., 13(3), 433-444, (2020).
[8] G. Yang, X. Zhai, Y. Li, B. Yao, Z. Ding, R. Deng, and Z. Zhang, Materials Letters, 242, 58-61, (2019); https://doi.org/10.1016/j.matlet.2019.01.102
[9] S. M. Camara, L. Wang, and X. Zhang, Nanotechnology, 24(49), 495401, (2013); https://doi.org/10.1088/0957-4484/24/49/495101
[10] L. Nie, J. Yang, D. Yang, S. Liu, Journal of Materials Science: Materials in Electronics, 30(4), 3760-3766, (2019); https://doi.org/10.1007/s10854-018-00658-2
[11] S. M. Pawar, B. S. Pawar, A.V. Moholkar, D.S. Choi, J.H. Yun, J. H. Moon, and J. H. Kim, Electrochimica Acta, 55(12), 4057-4061, (2010); https://doi.org/10.1016/j.electacta.2010.02.051
[12] Z. Xiao, S. Yu, Y. Li, S. Ruan, L. B. Kong, Q. Huang, and D. Tang, Materials Science and Engineering: R: Reports, 139, 100510518, (2020); https://doi.org/10.1016/j.mser.2019.100518
[13] H. Hussein, A. Yazdani, Materials Science in Semiconductor Processing, 91, 58-65, (2019); https://doi.org/10.1016/j.mssp.2018.11.005
[14] L. Glasser, and H.D.B. Jenkins, Journal of the American Chemical Society, 122(4), 632-638, (2000); https://doi.org/10.1021/ja992375u
[15] M. A. Ahmed, N. A. Bakr, and A. A. Kamil, Chalcogenide Letters, 16(5), 231-239, (2019).